Atmos. Meas. Tech. Discuss., 7, 7837–7882, 2014
www.atmos-meas-tech-discuss.net/7/7837/2014/
doi:10.5194/amtd-7-7837-2014

Atmospheric Measurement Techniques Discussions
Open Access

MISR Research Aerosol Algorithm: refinements for dark water retrievals

J. A. Limbacher[1,2] **and R. A. Kahn**[1]

[1]Earth Science Division, NASA Goddard Space Flight Center, Greenbelt, MD 20771, USA
[2]Science Systems and Applications Inc., Lanham, MD 20706, USA

Received: 19 May 2014 – Accepted: 8 July 2014 – Published: 31 July 2014

Correspondence to: R. A. Kahn (ralph.kahn@nasa.gov)

Published by Copernicus Publications on behalf of the European Geosciences Union.

Abstract

We explore systematically the cumulative effect of many assumptions made in the MISR Research Aerosol retrieval algorithm, with the aim of quantifying the main sources of bias and uncertainty over ocean, and correcting them to the extent possible. 1132 coincident, surface-based sun photometer spectral aerosol optical depth (AOD) measurements are used for validation. Based on comparisons between these data and our baseline case (similar to the MISR Standard algorithm, but without the "modified linear mixing" approximation), for mid-visible AOD < 0.10, a high bias of 0.024 (0.032 for blue) is reduced by about half in the blue and green bands when (1) ocean surface under-light is included and the whitecap reflectance is increased for the red band, (2) physically based adjustments in particle microphysical properties and mixtures are made, (3) an adaptive pixel selection method is used, (4) spectral uncertainty is estimated from vicarious calibration, and (5) minor radiometric calibration changes are made for the red and NIR wavelengths. Applying (6) more stringent cloud screening (setting the maximum non-clear fraction to 0.50) brings all median spectral biases below 0.01. Large surface-modeling uncertainties preclude the use of both the blue and green MISR bands for over-ocean aerosol retrievals, even at mid-visible AOD higher than 0.2. When all adjustments are included (except more stringent cloud screening) and a modified acceptance criterion is used, the RMSE decreases for all wavelengths by 10–26 % for the Research Algorithm itself, and 12–35 % compared to the Version 22 MISR Standard Algorithm (SA). At mid-visible wavelengths, 86 % of AOD data falls within 0.05 or 20 % of validation values; 61 % of blue band AOD data, and > 68 % of green, red, and NIR values fall within 0.03 or 10 %. For Ångström exponent (ANG): 68 % of 1117 validation cases for AOD > 0.01 fall within 0.275 of the sun photometer values, compared to 49 % for the SA. ANG RMSE decreases by 16 % compared to the SA, and the median absolute error drops by 36 %.

AMTD
7, 7837–7882, 2014

1 Introduction

The Research Aerosol Retrieval algorithm has been a workhorse for analyzing and interpreting multi-angle, multi-spectral data from the NASA Earth Observing System's Multi-angle Imaging SpectroRadiometer (MISR) instrument for over 15 years, and for investigating possible upgrades to the MISR operational aerosol algorithm (Kahn et al., 1998, 2001a). MISR measures upwelling short-wave radiance from Earth in four spectral bands centered at 446 (blue), 558 (green), 672 (red), and 866 nm (near-infrared, or NIR), at each of nine view angles spread out in the forward and aft directions along the flight path, at 70.5°, 60.0°, 45.6°, 26.1°, and nadir (Diner et al., 1998). The instrument samples a very large range of scattering angles – between about 60° and 160° at mid latitudes, providing information about aerosol microphysical properties. These views also capture air-mass factors ranging from one to three, offering sensitivity to optically thin aerosol layers, and allowing aerosol retrieval algorithms to distinguish surface from atmospheric contributions to the top-of-atmosphere (TOA) radiance.

The Research Algorithm (RA) is designed to provide flexibility in selecting (1) retrieval region spatial resolution, (2) components and mixtures to be included in the algorithm comparison-space aerosol climatology, and (3) acceptance criteria for retrieved aerosol amount and type, at the expense of the speed and autonomy required of the MISR Standard Operational Algorithm (SA). Early versions of the RA could analyze only single retrieval regions at a time (of any chosen pixel size), and could simulate only dark water surfaces of varying wind speed. Making use of recent advances in computer hardware and software technology, the MISR RA has been modified so it is practical to obtain results simultaneously for a number of retrieval regions within a geographic domain, while retaining flexibility in aerosol type and acceptance criteria options (e.g., Kahn and Limbacher, 2012).

Unlike the RA, the SA processes the entire MISR data record rapidly and autonomously, and includes an over-land retrieval component that self-consistently derives surface parameters along with overlying aerosol amount and type (Martonchik

AMTD
7, 7837–7882, 2014

et al., 1998, 2002; 2009). Later versions of the RA made it possible to input land-surface bi-directional reflectance distribution functions (BRDFs) derived from the SA, based on selecting low aerosol optical depth (AOD), seasonally equivalent cases from the time-series of SA data products (e.g., Chen et al., 2008).

This paper reports on upgrades to the MISR Research Aerosol Retrieval algorithm as they affect dark water retrievals. The changes are motivated in part to explore issues identified in recent validation analysis performed on the MISR Standard aerosol product (Kahn et al., 2010). The validation study showed, for example, that at low AOD, the V22 Standard product AOD tends to be overestimated, whereas at high AOD, the very limited number of over-ocean validation cases suggests the V22 product might be underestimated, relative to near-simultaneous surface-based sun photometer measurements. In the current paper, we examine in detail the quantitative effect of specific upgrades to the Research Algorithm on retrieved AOD and Ångström exponent (ANG). We implement and assess even minor adjustments that are justified on physical grounds, such as recent refinements to ocean surface whitecap spectral reflectivity and atmospheric gas spectral absorption parameters, with the understanding that the cumulative effects of even small corrections can be significant. Section 2 describes the latest implementation of the MISR dark water approach in the RA. Section 3 describes various modifications that are made to the algorithm based on theoretical or physical considerations. Section 4 describes empirical adjustments that are made to the algorithm, as well as AOD validation, ANG validation, and the effects of more stringent cloud screening. Conclusions are presented in Sect. 5.

2 MISR research retrieval dark water algorithm, and validation data

The essential aspects of the MISR Standard dark water retrieval algorithm are given in Martonchik et al. (1998, 2002) and Diner et al. (2008), and are similar to the historical implementation in the Research Algorithm (Kahn et al., 1998, 2001a). A flowchart outlining the steps involved in the aerosol retrieval over dark water for the Research

AMTD
7, 7837–7882, 2014

Algorithm is presented in Fig. 1. The most recent applications of the RA are closest to the SA version presented by Diner et al. (2008), with differences and new modifications as indicated below. Pre-processing of the MISR radiances in the RA includes converting radiance to equivalent reflectance, performing out-of-band spectral corrections, and making ozone, water vapor, and atmospheric gas polarization corrections as described in Kahn et al. (2001b, 2007), with minor net atmospheric gas optical depth increases compared to previous implementations of 0.0002 (blue), 0.0008 (green and red), and 0.0025 (NIR) based on refinements to the O_3 and H_2O_v spectra (http://spectralcalc.com).

2.1 Retrieval algorithm setup

In earlier versions of the RA, we represented the ocean surface as is done in the SA, with standard, wind-driven, isotropic surface roughness (Cox–Munk) and whitecap models, a glint exclusion angular region of about 40° around the specular direction, and an otherwise black surface in the MISR red and NIR bands at all viewing angles (e.g., Martonchik et al., 1998). At times, the RA also considered an isotropic (Lambertian) component of the reflection from within the water ("under-light"), using spectrally dependent albedo (A_0) values from ocean surface observations available at the time (Kahn et al., 2005a).

Initial comparisons of MISR coincidences with AERONET (Holben et al., 1998) and Marine Aerosol Network (MAN; Smirnov et al., 2009) surface-based sun photometer data indicated a high bias in MISR AOD when the total-column, mid-visible AOD fell below about 0.4 (Kahn et al., 2005b, 2010; Witek et al., 2013). This bias was present in both the SA and RA, although the greater variety of mixtures in the RA may have mitigated the bias in some cases. Three main factors can contribute to this issue: (1) instrument radiometric calibration, (2) the angularly dependent ocean surface reflectance (BRDF), and (3) the aerosol optical model adopted in the retrieval (type and vertical distribution), along with possible cloud contamination. The magnitudes of the contributions from these factors are expected to vary systematically with wavelength,

AMTD
7, 7837–7882, 2014

view angle, and environmental conditions, in ways that can help identify causes. For example, ocean color will have a larger impact at shorter wavelengths and near-nadir view angles, whereas the aerosol optical model is more likely to dominate at steeper view angles and higher AOD, and will depend on the dominant aerosol type in a given region.

When applying the RA, the radiative transfer code is run for an eight-dimensional space, covering ranges of viewing and solar geometry, AOD and aerosol mixture type, spectral band, surface atmospheric pressure, and for over-ocean retrievals, wind speed (Table 1). The wind speeds used in the RA come from the SfcWindsp dataset found in the MISR SA aerosol file, which are obtained from satellite scatterometer data specific to the day of the MISR observation. As with the SA, the radiative transfer result is referred to as the Simulated MISR Atmospheric Radiative Transfer (SMART) array (Diner et al., 2008). For a given retrieval, for each camera, values for the solar geometry, surface atmospheric pressure, and wind speed are linearly interpolated within the SMART array to the values appropriate to that case, reducing the dimensionality of the remaining space to four (mixture, AOD, spectral band, and camera). With the implementation of the RA used here, the AOD grid in the SMART array, which is at a coarse resolution (Table 1), is then interpolated using a cubic spline for each mixture, camera, and band, to produce simulated TOA reflectances on an adaptive mid-visible AOD grid of finer resolution.

The minimum AOD value for the adaptive grid is set to 0.0. To determine the maximum AOD value, first the largest possible AOD is estimated from the observed green-band TOA reflectances, separately for each aerosol mixture and each camera used, assuming the surface is dark water. To obtain the maximum green-band AOD for the retrieval overall, the smallest maximum AOD among the cameras is selected for each mixture, and then the maximum of these among all mixtures is the final choice. This process assures that a single camera contaminated with stray light does not skew the maximum AOD high, which could increase memory requirements and processing time unacceptably, while still retaining a liberal maximum-allowed value for the AOD. AOD

AMTD
7, 7837–7882, 2014

maxima in the other spectral bands are determined from the ratios of the spectral extinction cross-sections for each mixture.

With the minimum and maximum AOD established from the coarse SMART array, cubic splines are used to generate the finer grid in the AOD dimension for each aerosol mixture, camera, and band. If the maximum green-band AOD for the retrieval is below 0.15, we interpolate to a fine-grid spacing of ∼ 0.001 to achieve maximum AOD sensitivity; for AOD between 0.15 and 1.0, we interpolate to 0.002, and at higher maximum AOD, we use a grid of 0.005. Then the minima of a set of χ^2 test variables are assessed on this fine AOD grid for the AOD retrieval, separately for each mixture.

The χ^2 test variables are described in detail in previous papers (e.g., Kahn et al., 1998; Kahn and Limbacher, 2012). Briefly, the absolute χ^2 variable (χ^2_{abs}) is defined as:

$$\chi^2_{\text{abs}}[\text{mix, AOD}] = \frac{\sum_{\lambda,c} w \frac{(\rho-\rho_{\text{mod}})^2}{\rho^2_{\text{err}}}}{\sum_{\lambda,c} w} \quad (1)$$

The band and camera weights are represented by $w(\lambda, c)$, λ is the wavelength index, c is the camera index, ρ is the TOA observed reflectance, ρ_{mod} is the TOA modeled reflectance, mix is the aerosol mixture, AOD the AOD at which ρ_{mod} is assessed, and ρ_{err} is the total estimated uncertainty of the model/measurements (taken nominally as 5 % of the observed spectral reflectance value or 0.002, whichever is larger, but see Sect. 3.4 below). For each particular AOD and mixture, the χ^2 value is computed by performing the summation over all wavelengths and cameras used for the retrieval.

In addition to χ^2_{abs}, we obtain for each aerosol mixture the minimum value of the geometrically and spectrally weighted χ^2 variables (χ^2_{geom} and χ^2_{spec}, respectively), the maximum deviation among the terms in the χ^2_{abs} summation (χ^2_{maxdev}), as well as the maximum and mean of the triplet $\{\chi^2_{\text{abs}}, \chi^2_{\text{geom}}, \chi^2_{\text{spec}}\}$, called χ^2_{max3}, and χ^2_{mean3}, respectively (e.g., Kahn et al., 1998). This allows us to evaluate the efficacy of different acceptance criteria. Note that over ocean, acceptance criteria for aerosol mixtures and

AMTD
7, 7837–7882, 2014

AOD values are applied for the MISR red and NIR bands only, to minimize uncertainties based on the ocean surface modeling. The green and blue values are actually calculated for all cases, so we can assess the information content of the observations in those bands. Only cameras for which the MISR SA Retrieval Applicability Mask (retrAppMask) quality flag is 0, the glitter angle exceeds 40°, and the subregion is identified as being either inland water or deep ocean, are used for calculating the χ^2 metrics; mask values greater than 0 imply that glint, cloud, or cloud shadow could be an issue (e.g., Kahn et al., 2009).

The χ^2_{maxdev} variable is the largest term in the χ^2_{abs} summation (Eq. 1), and any mixture having a $\chi^2_{\text{maxdev}} > 10$ is eliminated. We then use χ^2_{abs} to constrain AOD over ocean, and unless specified otherwise, a χ^2_{abs} criterion is applied for the figures and results in this paper. For example, we accept all (mixture, AOD) pairs for which the residuals between the calculated and observed TOA equivalent reflectances fall within 1.5× chiMin of χ^2_{abs}, where chiMin is the lowest value, among all mixtures and AOD values in the algorithm climatology. Other acceptance criteria are discussed subsequently, as needed.

For the purpose of identifying possible camera or spectral-band-specific biases, we also save the AOD that corresponds to a residual ([model−observed reflectance]) value of 0.0 for each camera, band, and aerosol mixture. In general, the minimum absolute residual should be 0.0, unless the surface is very bright, or if the aerosol optical model is grossly incorrect. These AOD values correspond to the roots (zeros) of spline fits to the residuals on the coarse optical depth grid (defined in Table 1), specific to each camera, band, and mixture. We can then use constraints on aerosol type from the χ^2 tests, and by comparison with ANG values from coincident AERONET or MAN observations, to assess the individual camera and spectral band biases.

Our analysis approach uses coincident spectral AOD measurements from the AERONET (Holben et al., 1998) and MAN (Smirnov et al., 2009) sun photometer datasets for validation, interpolated to the MISR wavelengths, as in earlier work (e.g., Kahn et al., 2010). The RA code is run with varying assumptions and constraints, and the residuals are calculated for the validation cases, independently for each band and

AMTD
7, 7837–7882, 2014

camera. As a partial test of MISR-retrieved aerosol properties, we can also filter the data, keeping for example only those MISR-retrieved mixtures having Ångström exponents within 0.10 of the corresponding MAN/AERONET ANG derived from the interpolated MAN/AERONET AODs. Such constraints are available only at sun photometer sites; the cases rejected by this test highlight situations where providing external particle property information or assumptions would have the biggest impact on MISR retrieval quality.

2.2 MAN/AERONET-MISR data selection

For the present study, we use AERONET data that is spatially coincident with at least one pixel in a 3 × 3 MISR Standard retrieval region (each of which is 17.6 km in horizontal extent) and within ±1 h of the MISR overpass. For MAN data, we use ±30 min for the temporal constraint, due to generally greater temporal variability. The sun photometer data are then averaged over this window and interpolated to the four MISR wavelengths using a 2nd-order polynomial fit in log space. Additionally, for AERONET data we add the constraint that there be at least one AOD measurement on each side of the 1 h time window. For the entirety of this paper, we consider only dark-water MISR retrievals. The specific AERONET sites chosen were selected for consistency with previous work (Kahn et al., 2010), and to ensure that artifacts due to runoff, aerosol heterogeneity, and under-light are minimized.

Figure 2 shows the geographic distribution of the MAN/AERONET-MISR coincidences used for the current study. Our validation dataset includes only island AERONET sites (954 cases) plus 178 ship-based MAN cases, because the surfaces at these sites tend to be less polluted with run-off or biological activity than the more abundant AERONET coastal sites. Additionally, assuming that island sites are less likely to be major aerosol sources, the retrieved aerosol amount and type should be more homogeneous over a 3 × 3 retrieval-region area than at coastal sites. Table 2 lists the number of collocations conditioned on specific parameters. Using the MISR SA RetrAppMask quality flag (containing [16 × 16 pixels ×4 MISR bands × # of cameras used]

AMTD
7, 7837–7882, 2014

elements per retrieval), we designate a region as "clear" (a value of 0) if the mask identifies less than 5 % of the region as having a flag value greater than 0; i.e., at least 95 % of pixels pass all the radiance acceptance tests (e.g., Kahn et al., 2009), *not counting* those cameras entirely eliminated from consideration due to glint. (This condition removes 51 % of the validation cases. Note that over water, the SA requires only 12.5 % of pixels to have RetrAppMask = 0, but pixels eliminated due to glint are included in the SA assessment.) We designate a region as "not clear" if more than 5 % of pixels in the region have flag values greater than 0, i.e., fraction not-clear (FNC) > 0.05. Because we remove glint-contaminated cameras prior to running the RA, these flagged values should correspond primarily to clouds or cloud shadows (via the MISR SA brightness, direct cloud, angular smoothness or angular correlation masks; Martonchik et al., 2002). We also stratify by Chlorophyll *a* concentration (C), to identify regions where the surface under-light contribution might be important, based on spatially coincident data from MODIS-Aqua, SeaWiFS, and MERIS, merged by the GlobColour group using the Garver–Siegel–Maritorena (GSM) model (Maritorena and Siegel, 2005). Regions with average C values below 0.25 mg m^{-3} are characterized as low-C, whereas those with average C values above 0.50 mg m^{-3} are designated high-C. The data shown in Table 1 and Fig. 2 include all MISR-MAN/AERONET coincidences used in this study for which the MISR SA provides at least one valid dark-water retrieval.

2.3 The baseline case

We consider the data used to generate Figs. 3 and 4 to be the baseline cases, against which all other retrieval experiments are compared. The data used in these two figures were generated with the 74 aerosol-mixture climatology used in Version 22 of the SA (Kahn et al., 2010). The main difference between the SA and the RA as applied for Figs. 3 and 4 is that the modified linear mixing approximation (Abdou et al., 1997) is not used in the RA; instead, the full radiative transfer code is run for each mixture (see Sect. 2.4.2 below).

AMTD
7, 7837–7882, 2014

Figure 3 shows the MISR RA AOD bias relative to the sun photometer values, for each spectral band and camera, conditioned on various parameters. (All wavelengths are displayed in these plots to the extent possible.) Figure 3a includes all coincidences in the baseline comparison data set. Figure 3b is stratified to include mostly clear retrieval regions (FNC < 0.05), with low-C ($C \leq 0.25$) and low AOD (AOD ≤ 0.10). Note that the red-channel retrieved AOD has a small high bias in AOD for most cameras (∼ 0.01), whereas the NIR band has a small low bias in AOD for the near-nadir cameras (< 0.01). Figure 3c is the same as 3b, except that AOD ≥ 0.20. The green band has a much lower bias compared to Fig. 3b, but it is still biased high (∼ 0.02 on average). The red and the NIR bands are both biased low by about 0.01 for most cameras. The fourth plot shows the AOD bias in regions with either higher chlorophyll content ($C \geq 0.50$) or higher non-clear fraction (FNC ≥ 0.75). As expected, this leads to high bias in retrieved AOD for all bands and cameras (0.27 for blue, 0.08 for green, ∼ 0.03 for red, and ∼ 0.02 for NIR).

Figure 4 (and Table 5) show the MISR Research Retrieval AOD results compared to AERONET/MAN for the baseline case at all four wavelengths. Note that > 70 % of the RA results, using the 74-aerosol-mixture climatology of the SA but without the modified linear mixing approximation, fall within the 0.05 or 20 % AOD uncertainty envelope for all wavelengths, and > 80 % for all but the blue band. This is comparable to (∼ 5 % better than) the result for a broader set of Maritime cases assessed with the SA by Kahn et al. (2010). The results (both ANG and spectral AOD) for the SA are also shown in Table 5, Figs. 10 and 11.

3 Algorithm modifications based on physical considerations

This section describes the impact on retrieved AOD of individual modifications to the way (1) observed reflectances over a retrieval region are selected, (2) the ocean surface is modeled, (3) the aerosol components and mixtures are defined, and (4) the measurement uncertainty is assessed in the calculation of the retrieval acceptance

AMTD
7, 7837–7882, 2014

test variables. These changes are motivated by physical considerations described in each subsection.

3.1 Selection of TOA reflectances

When comparing with SA results over ocean, for the nominal case we select the same MISR reflectances for the RA as used by the SA, i.e., for each 1.1 km pixel within the retrieval region that passes the SA cloud contamination, shallow water, and other tests (Kahn et al., 2009), the reflectances in the red and NIR bands for all available cameras are averaged, and the darkest pixel is taken as representing the 16 × 16 pixel retrieval region. As such, red band contributions generally dominate over dark water, because dark water tends to be brighter at shorter wavelengths. However, at other times we adopt alternative strategies for the RA, such as (1) taking the darkest pixel channel-by-channel, or (2) making a selection based on the histogram of reflectances over the useable pixels in the entire retrieval region, as is done for MODIS (e.g., Remer et al., 2005). We also examined an approach that takes account of scene attributes that vary with AOD and cloud fraction.

When scene variability is dominated by something other than aerosol, i.e., at low AOD or high non-clear fraction, the retrieval is more likely to contain surface or cloud artifacts, respectively, that can increase the observed TOA reflectance. So for this experiment, if green band AOD < 0.35 (based on the darkest pixel) or FNC ≥ 0.10 for the region, we select the minimum reflectance pixel over a 17.6 km × 17.6 km retrieval region independently for each spectral band and camera, under the assumption that the aerosol is uniform over the retrieval region.

At higher AOD, aerosol variability is likely to become important, so the darkest pixel might not best represent retrieval-region reflectance as a whole, especially if, at the same time, FNC is very low. So if the green band AOD ≥ 0.35 (determined by using the minimum reflectance pixel with the traditional χ^2 metric) and FNC ≤ 0.10 for the region, we select the median reflectance pixel over the 17.6 km × 17.6 km retrieval region, independently for each spectral band and camera. If 0.0 < FNC < 0.10, we take

AMTD
7, 7837–7882, 2014

a linear weighting of the median reflectance pixel and the minimum reflectance pixel. So, for example, at FNC of 0.025, the total reflectance would be the sum of 25 % of the minimum reflectance pixel plus 75 % of the median reflectance pixel.

The scatter-density plot for the RA when the median-or-minimum approach is applied looks very similar to the baseline case and is not shown, but the quantitative differences are given in Table 5. The alternative pixel selection incrementally reduces the retrieved AOD Root-Mean-Square-Error (RMSE) by 5–10 %, the median bias decreases by 10–20 % in all bands, and there are fewer outliers for these cases.

3.2 Ocean surface model

Here we expand on previous work by accounting for the two dynamic components of under-light (and surface whitecaps), as discussed in Sayer et al. (2010). We consider this ocean surface model as a limiting case, to explore the degree to which the factors involved might affect AOD retrieval quality. Contributions to the changing under-light can come from (1) colored dissolved organic matter and detrital organic materials absorption (CDM) and (2) Chlorophyll *a* (*C*). We use the GlobColour GSM monthly ocean color products (Barrot et al., 2010), taking the high-resolution (4.4 km) *C* and CDM values nearest to the center of the MISR retrieval region. If the region has no valid monthly values for either *C* or CDM, we use default values of $\sim 0.01\,\mathrm{m}^{-1}$ (558 nm) for the CDM absorption coefficient and 0.20 for the Chlorophyll *a* concentration. The contribution of molecular scattering (of water) is also included in the under-light model (details can be found in Sayer et al., 2010). Recent measurements also report on the angular dependence of the ocean surface reflectance (e.g., Voss and Chapin, 2005; Antoine et al., 2013). However, it is not clear how general these results might be, so including this refinement is beyond the scope of the current study; having additional constraints on ocean surface BRDF would be an asset to multi-angle remote sensing of Earth's surface.

The whitecap model used by the current Standard and baseline Research Algorithms assumes a spectrally invariant albedo of 0.22 from Koepke (1984), with

AMTD
7, 7837–7882, 2014

wind-speed-dependent whitecap coverage from Monahan and O'Muircheartaigh (1980). We adopt alternative albedo values of 0.40 for the blue and green, 0.36 for red, and 0.24 for NIR, based on Frouin et al. (1996) and consistent with Sayer et al. (2010).

In Fig. 5 we quantify the channel-by-channel differences that the addition of under-light and the updated whitecap albedo values make to the AOD retrievals for all the validation data cases, when the retrieved aerosol mixture is the same for all channels, but the AODs are retrieved for each band and camera separately. The AOD bias in the blue and green drops substantially when under-light and updated whitecaps are included, compared to the baseline case shown in Fig. 3a (blue decreases by ~ 0.1 and green decreases by > 0.03); the AOD bias in the red drops by a much smaller absolute amount (0.004), and the NIR increases slightly (0.003). The slight NIR increase is due to changes between Figs. 3 and 5 in the mixtures selected (the retrieved particle size increases, retrieved ANG decreases). If the mixtures chosen for the ocean-surface-model retrievals were identical to the baseline case, the red AOD bias would decrease by ~ 0.007 and the NIR would decrease by ~ 0.0007. Also, because we do not use either the blue or green bands for our retrievals, the large bias that still exists at those two wavelengths remains an assumption based on the selected aerosol optical model rather than an AOD retrieval result. For the actual AOD retrievals, the RMSE of the aggregate data is shown in Table 5; compared to Fig. 4, the AOD discrepancies change by −9 %, −6 %, −5 %, and 0 % for the blue, green, red, and NIR bands due to the surface model refinements. The statistics of the AOD and also the ANG retrievals for the surface model adjustment are shown in Table 5.

3.3 Aerosol components and mixtures

The Version 22 MISR SA aerosol type climatology has been assessed in light of aerosol particle properties measured during field campaigns and aggregated from surface network observations (Kahn et al., 2010; Kahn and Gaitley, 2014). Components and mixtures included in the RA are informed by these results, as well as by additional sensitivity analysis summarized here.

AMTD
7, 7837–7882, 2014

3.3.1 Real part of refractive index

Particle property retrievals are multi-dimensional, and early sensitivity studies showed no ability to constrain the real part of the refractive index (n_r) from MISR data alone, due to uncertainties in the retrieved values of better-constrained variables (Kahn et al., 1998; Chen et al., 2008). As such, the MISR SA Version 22 (and previous versions) arbitrarily assumed a fixed value of n_r for all spherical particles of 1.45. However, despite low retrieval sensitivity, the selected value of n_r affects the retrieved AOD. Specifically, an overestimated n_r in the retrieved particle type compared to the actual atmosphere, with other factors fixed, produces a systematically reduced value of retrieved AOD, and conversely. Essentially, as n_r increases, other things being equal, the curvature of the particle single-scattering phase function $P(\theta)$ (where θ is the scattering angle) increases, directing a larger fraction of scattered light into the backward directions where MISR observes. So as n_r increases, less AOD is required to match the observed reflectance, producing lower retrieved AOD, and conversely. For larger sea-salt particles in particular, n_r is typically around 1.37, closer to the value for pure water (1.33) than to 1.45 (e.g., Dubovik et al., 2002; Smirnov et al., 2003). Here we adopt n_r of 1.37 for the 1.28 and 2.80 micron r_e spherical sea-salt and other hydrated aerosol optical analogs in a 774-mixture RA particle climatology. We use this larger climatology as an alternative to the 74-mixture set from the V22 MISR SA that was applied in the baseline case; Table 3 lists the alternative components and their key optical properties, and Table 4 summarizes the mixtures included in the validation section. Figure 6 demonstrates how overestimating the real part of the refractive index can lead to retrieved-AOD underestimation. The top four plots in Fig. 6 show the retrieved AOD fractional error when the simulated atmosphere contains 1.28 micron non-absorbing particles with $n_r = 1.37$, and the comparison space contains 1.28 micron non-absorbing particles but with $n_r = 1.45$, for a range of observational geometries and AOD values (a fractional error of −0.2 indicates underestimation by 20 %). Note that overestimating n_r can lead to large negative biases regardless of the absolute AOD. In the case of our 1.28 micron

AMTD
7, 7837–7882, 2014

coarse-mode particle, the change from $n_r = 1.45$ to 1.37 results in a ~25 % increase in retrieved AOD. The second row in Fig. 6 illustrates how little sensitivity the retrieval has to n_r; although the fractional deviations are high, the absolute χ^2 values are low (generally < 1.0), highlighting the need for the assumed n_r values to be as close to the natural values as possible. Overall, the sensitivity of retrieved AOD to the value of n_r assumed in the climatology tends to peak for particles having effective radius (r_e) between about 0.25 and 1.3 microns for most MISR observing geometries, based on additional sensitivity analysis (additional results presented in Supplement).

3.3.2 Component particle optical analogs, mixtures, and mixing rules

Following Kahn et al. (2010), we add to the RA climatology spherical aerosol components having r_e of 0.57 and 1.28. We also add cirrus optical analogs (Pierce et al., 2010), smoke and pollution analogs (having spectrally steep and flat particle absorption, respectively), and mixtures containing both dust and smoke analogs. These represent aerosol types present in the atmosphere but lacking from the V22 SA climatology. The components used for the current analysis are summarized in Table 3.

Taking all combinations of components 1, 2, and 3 in Table 4, in increments of 10 % green-band AOD contribution, with repeated mixtures removed, creates most of the aerosol mixtures used for this study. In addition, we allow the lowest non-zero contribution of each component particle to be 5 %, and adjust the other components accordingly. Cirrus particles are not mixed with other species in the column, as this would require including aerosol layers at different elevations in the radiative transfer code, which is beyond our current capabilities. Because there are fewer operational demands on the RA than on the SA, we can afford to characterize aerosol mixtures optically by combining the phase functions of the components before running the radiative transfer code, according to:

$$P_{\mathrm{mix}}(\Theta,\lambda) = \sum_n P_n(\Theta,\lambda)\cdot f_n(\lambda)\cdot \mathrm{SSA}_n(\lambda) \quad (2)$$

AMTD
7, 7837–7882, 2014

SSA_n is the spectral single-scattering albedo of component n of the mixture, representing the scattered fraction of light extinction by that component, P is the particle spectral single-scattering phase function, f_n is the spectral fractional AOD contribution of the particle at wavelength (λ), and Θ is the scattering angle. $P_{\text{mix}}(\Theta,\lambda)$ is normalized by fitting a 5th order spline in cos(Θ) space to $P_{\text{mix}}(\Theta,\lambda)$, integrating the spline from −1 to 1 and scaling $P_{\text{mix}}(\Theta,\lambda)$ to 2. This avoids the assumptions involved in the Modified Linear Mixing (MLM) approach employed in the Standard Algorithm (Abdou et al., 1997), which can cause substantial high AOD biases, especially when components having significantly different sizes or SSA values are mixed at high AOD. Figure 7 illustrates the situation for a two-particle mixture; orbit-average retrieved-AOD differences can be as large as 10 % for the cases shown, and the differences depend on observing geometry, as well as both the size and SSA differences between the two components. The major cost of eliminating MLM is the size of the Look-Up-Tables (LUT) required. For 774 mixtures, the LUT is ∼ 8 GB in size. The statistics of the AOD and ANG retrievals for the 774-mixture set are shown in Table 5. It is clear from Table 5 that the addition of the 774 mixtures results in improved AOD retrievals in both the blue and green, as well as significantly improved ANG retrievals. (Retrievals based on linear mixing and on modified linear mixing are compared to retrievals using combined phase functions (Eq. 2) over a broad range of the particle size and SSA options in the Supplement.)

3.4 Spectral measurement uncertainty estimation

Somewhat arbitrarily, we previously set the reflectance measurement uncertainty estimates for the χ^2 test variables (e.g., ρ_{err} in Eq. 1) equal to 5 % of the reflectance value or 0.002, whichever is larger. Here we estimate the actual spectral reflectance measurement uncertainty, making use of the validation data sets and the aggregate of adjustments and corrections described above, as well as a calibration adjustment discussed in Sect. 4.1, with the following uncertainty metric, evaluated separately for each camera and spectral band:

AMTD
7, 7837–7882, 2014

$$\varepsilon = \frac{\sum_{\text{mix}} \frac{|\rho - \rho_{\text{mod}}|}{\rho}}{n_{\text{mix}}} \quad (3)$$

Here ρ is the TOA reflectance observed by MISR, and ρ_{mod} is that calculated with the forward radiative transfer code for each mixture that passes the χ^2_{abs} acceptance criterion, using the AERONET/MAN spectral AOD values as constraints (Fig. 1, middle branch).

Figure 8 shows the 68th percentile values of the camera and band-specific aggregated reflectance uncertainty metric (Eq. 3) when all validation cases are considered. These uncertainty values include any error due to uncertainty in the optical modeling (i.e., representations of particle scattering, absorption, and vertical distribution, scene polarization, the ocean surface, etc.), any error due to uncertainty in the MISR radiometric calibration, as well as discrepancies caused by error inherent in the MAN/AERONET data. It is important to note that even though the relative error appears to be quite large for the red and NIR bands, the median absolute error, $|\rho - \rho_{\text{mod}}|$, is only ~ 0.004 for these bands (~ 0.002 for NIR in the nadir camera), compared to 0.005 for the green, and 0.012 for the blue, averaged over all nine cameras (plot not shown). Because ρ_{err} should only include MISR model/measurement uncertainty, these plots provide a crude upper bound on the desired quantity. Based on this analysis, we alternatively set ρ_{err} for the χ^2 tests equal to $\max[0.01, \rho]$ multiplied by 0.05, 0.04, 0.055, 0.08, for blue, green, red and NIR bands. We find that applying this minimum uncertainty formulation gives more appropriate relative weight to the NIR band in the total χ^2 calculation over water, i.e., greater weight at low AOD and lower weight at high AOD. These changes also resulted in the loss of $\sim 1\,\%$ of 3×3 data regions used in the analysis because small deviations in the NIR at low AOD result in high χ^2 values. The factors calculated here apply to dark water surfaces; multipliers would have to be derived from appropriate validation cases for other surface types.

AMTD
7, 7837–7882, 2014

4 Algorithm empirical adjustments and validation

In this section we assess the cumulative effect of the algorithm modifications based on physical considerations described in Sect. 3. But in addition to these modifications, our validation data allow us to make some empirical adjustments to factors in the algorithm for which existing physical constraints are loose. This includes the stringency with which we apply cloud screening, and band-to-band calibration within the ∼ 1.5 % accuracy to which it is determined by formal instrument calibrations procedures (Bruegge et al., 2007).

4.1 Calibration adjustments based on Ångström exponent comparisons

Figure 9a and b shows a large (∼ 0.20) negative bias in the retrieved ANG compared to the validation data for AOD > 0.20, even though all the spectral adjustments to the retrieval assumptions have been made (excluding the reflectance uncertainty adjustments of Sect. 3.4). This leaves tiny adjustments to the relative radiometric calibration (< 1 %) in the red and NIR bands as possible corrections, given the great sensitivity of ANG to small changes in these quantities. We find that increasing the MISR red band radiances by 0.75 % and lowering the NIR band radiances by 0.75 % creates both better agreement for all wavelengths, and a substantially lower-magnitude bias in the retrieved ANG for both MISR-MAN coincidences and MISR-AERONET coincidences. This adjustment causes the ANG RMSE to decrease by more than 20 % for both datasets at high AOD (> 0.20), and results in an ANG bias that is less than 0.10 in magnitude. Figure 9c and d shows improved ANG slopes due to the reflectance uncertainty adjustment described in Sect. 3.4. Any further adjustment to the radiometric calibration would create greater positive bias in ANG for some of the low AOD bins (Fig. 10b). Although we find that modifying the calibration of the red and NIR bands can bring the retrievals into better alignment with AERONET/MAN, we are not drawing any conclusions about the radiometric calibration of MISR itself. Other factors, such as

AMTD
7, 7837–7882, 2014

particle-model errors, surface-representation errors, uncorrected scene polarization, etc. could contribute to biases in RA-retrieved ANG.

4.2 Ångström exponent validation and adaptive χ^2 selection criterion

ANG validation against AERONET/MAN is shown in Fig. 10a. The second line in the triplet series of whiskers (SA, RA-baseline, RA-modified) was generated with the traditional $\min(\chi^2_{\text{abs}}) \cdot 1.5$ mixture acceptance metric used previously, whereas the third whisker was created using a different criterion involving χ^2_{abs}. This alternative criterion is $\min(\chi^2_{\text{abs}}) + 0.35$ for AOD = 0.0 and $\min(\chi^2_{\text{abs}}) \cdot 1.5$ for AOD $\geq$ 0.20, with a linearly weighted value for AODs between 0.0 and 0.20. This results in 68th percentile values (for the seven lowest AOD bins) that are $\sim$ 10 % lower than the standard $\min(\chi^2_{\text{abs}}) \cdot 1.5$. Because AODs are not negatively affected by this adaptive χ^2 criterion, and the use of an absolute criterion makes sense at low AOD due to the limits of measurement sensitivity to particle properties in this regime (e.g., Kahn et al., 2011), we use the new technique for the remainder of the paper.

Figure 10a (and Table 5) show that the MISR RA sensitivity to ANG improves dramatically as AOD increases, as expected (Kahn et al., 2010; Kahn and Gaitley, 2014), with 68th percentile values of ANG statistical discrepancy dropping from $\sim$ 0.50 at an AOD of $<$ 0.04 down to $\sim$ 0.24 for AODs between 0.08–0.095. ANG sensitivity continues to improve as AOD increases, with 68th percentile values dropping further, to $\sim$ 0.18, for AOD $>$ 0.35. Correlation and slope also improve with increasing AOD (see Fig. 9c and d). Figure 10b shows a scatter plot of MISR RA ANG (computed using the mean spectral extinction cross-section ratios) vs. AERONET/MAN ANG for all AOD $>$ 0.01. Overall, 68 % of the MISR RA ANG values fall within 0.275 of the MAN/AERONET ANG value.

Figure 10a (left whisker in triplet) and c (also Table 5) shows ANG, calculated from the SA AOD retrievals, compared to AERONET/MAN. We computed these ANGs from the SA-retrieved best-estimate spectral AODs, which represent the mean spectral AOD

AMTD
7, 7837–7882, 2014

of all passing mixtures. This makes our definition of ANG (for the SA) identical to the one for the SA (best-estimate ANG) (Bull et al., 2011). We use the extinction cross-section ratios to compute ANG for the RA rather than the spectral AODs because we allow the RA to select 0.0 for the minimum AOD, which would otherwise complicate the ANG calculation. Compared to the SA, there is clear improvement in the median-absolute-error (drops by 36 %), RMSE (drops by 16 %), and correlation (increases by 0.04). Slope improves by ~ 0.10 for AOD > 0.16 (not shown), and the median bias is much lower in magnitude for all AODs. Before modifying the χ^2 acceptance criterion, the SA-retrieved ANG more closely matched AERONET/MAN ANG values at low AOD, possibly owing to the fact that only 74 aerosol mixtures are employed, vs. the 774 used for the RA. Because the RA is likely not sensitive to all of these mixtures at low AOD, increasing the number of mixtures selected (which is what occurs at low AOD with the larger mixture climatology and χ^2 criterion modification) tends to reduce outliers, increase the correlation, and decrease the slope. As AOD approaches 0.20, the impact of this modification diminishes, and the greater variety of aerosol models allows for a more robust ANG retrieval. It is likely that external constraints are needed to winnow down the passing-mixture list at low AOD, such as using a aerosol transport model to select among the list of passing mixtures (e.g., Kahn, 2012; Li et al., 2014), as the information content of the MISR radiances tends to be swamped by surface effects and Rayleigh scattering signals under these circumstances.

4.3 AOD validation

Figure 11 and Table 5 show the aggregated effects of the median-or-min reflectance selection approach, under-light + updated whitecaps, updated n_r, new mixtures, and the calibration adjustment, as well as the effect of using the modified χ^2_{abs} metric described in Sect. 4.2. Taken together, the aggregated changes compare favorably relative to the RA baseline case shown in Table 5, with RMSE decreases of 26, 20, 16, and 10 % for blue, green, red, and NIR, respectively. For the RA over dark water, 61, 67, 72, and

AMTD
7, 7837–7882, 2014

74 % of retrievals fall within ∼ 0.03 or 10 % of the validation AOD values in the blue, green, red, and NIR bands.

Table 5 also gives the results of the MISR SA AOD for the same sites and same retrieval regions used for the RA. Compared to the SA, the upgraded RA RMSE drops by 35, 27, 21 and 12 % in the blue, green, red, and NIR bands. The fraction of AOD retrievals meeting 0.03 or 10 % of the validation AOD values changes by +0.24, +0.16, +0.10 and +0.05. The correlation (r) between the SA and AERONET/MAN is ≥ 0.94 at all wavelengths, and is ≥ 0.96 for the RA. The slope for the SA is greater than 0.97 for all wavelengths, and the slope for the RA increases from 0.88 in the blue to 0.97 in the NIR. The reason the RA vs. AERONET/MAN AOD slope is smaller for the RA than the SA at shorter wavelengths is related primarily to poor constraints on aerosol type in the presence of the larger algorithm aerosol climatology; most of the discrepancy between SA and RA slopes is removed for AOD > 0.20. However, the aggregated adjustments to the RA produce substantial statistical improvements to the retrieved spectral AOD even at low AOD.

Figure 11 shows the error statistics of |MISR-AERONET/MAN| spectral AOD for different AOD regimes. This figure demonstrates that the RA performs better than the SA over most AOD bins (and wavelengths). The largest improvements are seen at both very low AOD (< 0.10) and at higher AOD (≳ 0.35), as well as at shorter wavelengths.

4.4 Enhanced cloud screening

Figure 11 and Table 5 also show the effect of applying a maximum NCF of 0.50 to the RA with all adjustments described above applied, and to the SA. This is similar to what is done by Witek et al. (2013), except that we do not consider glint-contaminated cameras in the NCF calculation. Note that this removes an additional 13 % of 3 × 3 retrieval regions (as compared to a much higher fraction for Witek et al., 2013). However, the 0.01 AOD bias that was present at all wavelengths is now reduced to ≤ 0.005 for all wavelengths. Every statistic except slope improves when the NCF is applied (Table 5). The Standard Algorithm AOD retrieval sees a greater improvement than the Research

AMTD
7, 7837–7882, 2014

Algorithm with this adjustment, which is likely due to the SA having poorer statistics overall to begin with. The high bias in AOD still exists in every wavelength (~ 0.032 for blue, ~ 0.007 for NIR), but is reduced by ~ 0.006. Interestingly, setting the NCF to 0.50 had virtually no effect on the retrieved ANG statistics (RMSE, MAE), except for the slope, which increased from 0.499 to 0.536, likely due to preferential removal of larger cloud droplets and/or larger, hydrated particle contributions. This also occurs for the SA, with the slope increasing from 0.495 to 0.521.

Shi et al. (2014) used MODIS cloud-detection products that make use of spectral channels at longer wavelengths than those available on MISR, to screen for clouds in coincident MISR aerosol retrievals. They identify a probable thin cirrus contribution averaging about 0.01 to the AOD retrievals over ocean, and larger effects in the vicinity of cloud edges. It is beyond the scope of the current paper to include MODIS cloud masking, but overall, the implementation of a maximum non-clear fraction even within the MISR products alone results in a large improvement to the Standard Algorithm (as also shown by Witek et al., 2013), and a more modest improvement to the Research Algorithm results.

5 Conclusions

In this paper, we assess the impacts of changes to the MISR Research Aerosol Retrieval algorithm over water, modifications based on physical considerations, as well as empirical adjustments that improve comparisons with validation data and fall within the range of allowed values based on all other available constraints. In the process, we assess the impact on retrieved AOD of several assumptions commonly employed in aerosol remote sensing, and some assumptions that are specific to the MISR Standard Algorithm. We accomplish this by systematically altering the algorithm such that each modification is performed independently, and the results are compared against more than 1100 MAN-AERONET coincident, dark-water observations.

AMTD
7, 7837–7882, 2014

We show that the cumulative effect of several physically motivated changes eliminates about half the statistical bias in the retrieved AOD. Specifically, (1) the small increase in TOA model reflectance in the red band produced by including spectral under-light contributions causes the retrieved red band AOD to drop relative to the NIR, resulting in the algorithm systematically selecting larger particles. The consequent reduction in ANG reduces the retrieved mid-visible AOD bias and improves the ANG correlation. (2) Correcting the n_r value assumed for hydrated particle optical models can increase retrieved AOD at all AOD values, by up to 25 % if the retrieved particle is large. (3) Removing the linear mixing approximation reduces AOD overestimation at all AODs, but especially at higher AOD. (4) An adaptive pixel selection technique is introduced that minimizes the effects of unmasked cloud at low AOD, and of aerosol variability at high AOD. For the RA, this change causes spectral AOD RMSE to decrease by 5–10 %. And (5), in Sect. 3.3.2, we show the impact of including a greatly expanded mixture list, which causes the AOD RMSE to change by −17 % to +2 %, with the increase occurring in the NIR, where the statistics were already much better than the other bands before this adjustment was applied.

All modifications are then aggregated and an error analysis is performed to produce an empirical estimate the reflectance uncertainty, used for the χ^2 calculations. A spectrally invariant uncertainty of 5 % was previously assumed for both the MISR Standard and Research Algorithms. However, the relative uncertainty is much higher in the NIR than the red band, which is especially important for over-water retrievals. In addition, the minimum value used for the χ^2 uncertainty was too large for the NIR, which caused less weighting to be assigned to the NIR band than was appropriate at low AOD. After making all corrections, small calibration adjustments of +0.75 % and −0.75 % were applied to red and NIR reflectances, respectively, to bring ANG into substantially better agreement with AERONET without significantly affecting AOD performance.

Applying all these physically based and empirical adjustments decreased AOD RMSE by 10–26 % compared to the algorithm before any corrections were implemented, and an RMSE decrease of 12–35 % compared to the SA. ANG RMSE dropped

AMTD
7, 7837–7882, 2014

by 16 % compared to the SA, and MAE decreased 36 %. Enhanced cloud-screening, implemented by setting a non-clear fraction maximum of 50 %, brought the spectral AOD bias to under 0.005, and greatly reduced the number of outliers, while only removing 13 % of 3 × 3 retrieval regions.

These results make clear that adding a relatively simple under-light model, modifying particle properties to be more realistic, introducing a comprehensive mixture list, and (in the case of the Research Algorithm) making a small calibration correction can dramatically improve aerosol retrievals.

Other factors that remain to be considered include: (1) the angular dependence of ocean surface reflectance (BRDF), (2) the coupled impact of polarization and uncertain aerosol vertical distribution on the retrieved quantities, which could be significant for over-ocean transported aerosol residing in the free troposphere, and (3) the use of an aerosol transport model or other external source to constrain aerosol type when many mixtures pass the algorithm acceptance criteria, e.g., frequently at low AOD. However, at least based on the 1132 over-ocean validation cases included here, the adjustments applied here are sufficient to remove nearly all the apparent bias in both AOD and ANG.

The updated MISR RA (with all of the corrections made) will continue to serve as our platform for testing retrieval ideas, and for extracting the maximum particle type information on a case-by-case basis for local and regional-scale studies. However, to take advantage of these improvements for global-scale applications, the adjustments demonstrated here must be implemented in an operational code, a non-trivial task in itself.

The Supplement related to this article is available online at doi:10.5194/amtd-7-7837-2014-supplement.

Acknowledgements. We thank our colleagues on the Jet Propulsion Laboratory's MISR instrument team and at the NASA Langley Research Center's Atmospheric Sciences Data Center for

AMTD
7, 7837–7882, 2014

MISR Research-Aerosol-Algorithm: refinements for dark water retrievals

J. A. Limbacher and R. A. Kahn

their roles in producing the MISR data sets, and our colleagues at the NASA Goddard Space Flight Center, the SeaWiFS, MERIS, and MODIS ocean color teams, the ESA, the GlobColour group, Brent Holben and the AERONET team, and Alexander Smirnov and the MAN team for the invaluable data sets they produce. We also thank Sergey Korkin, Alexei Lyapustin, Leigh Munchak, Falguni Patadia, and Andrew Sayer for helpful discussions, and Maksym Petrenko for identifying the MISR/MAN coincidences. This research is supported in part by NASA's Climate and Radiation Research and Analysis Program under H. Maring, NASA's Atmospheric Composition Program under R. Eckman, and the NASA Earth Observing System MISR instrument project.

References

Abdou, W. A., Martonchik, J. V., Kahn, R. A., West, R. A., and Diner, D. J.: A modified linear-mixing method for calculating atmospheric path radiances of aerosol mixtures, J. Geophys. Res., 102, 16883–16888, doi:10.1029/96JD03434, 1997.

Antoine, D., Morel, A., Leymarie, E., Houyou, A., Gentili, B., Victori, S., Buis, J.-P., Buis, N., Meunier, S., Canini, M., Crozel, D., Fougnie, B., and Henry, P.: Underwater radiance distributions measured with miniaturized multispectral radiance cameras, J. Atmos. Ocean. Tech., 30, 74–95, 2013.

Barrot, G., Mangin, A., and Pinnock, S.: GlobColour Product User Guide, available at: http://www.globcolour.info (last access: 31 January 2014), 2010.

Baum, B., Yang, P., Heymsfield, A., Platnick, S., King, M., Hu, Y., and Bedka, S.: Bulk scattering properties for the remote sensing of ice clouds: Part II. Narrowband models, J. Appl. Meteorol., 44, 1896–1911, doi:10.1175/JAM2309.1, 2005.

Bruegge, C. J., Diner, D. J., Kahn, R. A., Chrien, N., Helmlinger, M. C., Gaitley, B. J., and Abdou, W. A.: The MISR radiometric calibration process, Remote Sens. Environ., 107, 2–11, doi:10.1016/j.rse.2006.07.024, 2007.

Bull, M., Matthews, J., McDonald, D., Menzies, A., Moroney, C., Mueller, K., Paradise, S., and Smyth, M.: MISR Data Products Specifications Revision S, available at: https://eosweb.larc.nasa.gov/project/misr/dps (last access: 2 March 2014), 2011.

AMTD
7, 7837–7882, 2014

Chen, W.-T., Kahn, R. A., Nelson, D., Yau, K., and Seinfeld, J.: Sensitivity of multi-angle imaging to optical and microphysical properties of biomass burning aerosols, J. Geophys. Res., 113, D10203, doi:10.1029/2007JD009414, 2008.

Diner, D. J., Beckert, J. C., Reilly, T. H., Bruegge, C. J., Conel, J. E., Kahn, R. A., Martonchik, J. V., Ackerman, T. P., Davies, R., Gerstl, S. A. W., Gordon, H. R., Muller, J.-P., Myneni, R., Sellers, R. J., Pinty, B., and Verstraete, M. M.: Multiangle Imaging SpectroRadiometer (MISR) description and experiment overview, IEEE T. Geosci. Remote, 36, 1072–1087, 1998.

Diner, D. J., Abdou, W. A., Ackerman, T. P., Crean, K., Gordon, H. R., Kahn, R. A., Martonchik, J. V., Paradise, S. R., Pinty, B., Verstraete, M. M., Wang, M., and West, R. A.: Multi-angle Imaging SpectroRadiometer Level 2 Aerosol Retrieval Algorithm Theoretical Basis, Revision G, Jet Propulsion Laboratory, California Institute of Technology JPL D-11400, Pasadena, California, USA, 2008.

Frouin, R., Schwindling, M., and Deschamps, P.-Y.: Spectral reflectance of sea foam in the visible and near-infrared: in situ measurements and remote sensing implications, J. Geophys. Res., 101, 14361–14371, doi:10.1029/96JC00629, 1996.

Holben, B. N., Eck, T. F., Slutsker, I., Tanre, D., Buis, J. P., Setzer, A., Vermote, E., Reagan, J. A., Kaufman, Y. J., Nakajima, T., Lavenu, F., Jankowiak, I., and Smirnov, A.: AERONET – a federated instrument network and data archive for aerosol characterization, Remote Sens. Environ., 66, 1–16, 1998.

Kahn, R. A.: Reducing the uncertainties in direct aerosol radiative forcing, Surv. Geophys., 33, 701–721, doi:10.1007/s10712-011-9153-z, 2012.

Kahn, R. A. and Gaitley, B. J.: An analysis of global aerosol type as retrieved by MISR, J. Geophys. Res., submitted, 2014.

Kahn, R. A., Banerjee, P., McDonald, D., and Diner, D.: Sensitivity of multiangle imaging to aerosol optical depth, and to pure-particle size distribution and composition over ocean, J. Geophys. Res., 103, 32195–32213, 1998.

Kahn, R. A., Banerjee, P., and McDonald, D.: The sensitivity of multiangle imaging to natural mixtures of aerosols over ocean, J. Geophys. Res., 106, 18219–18238, 2001a.

Kahn, R. A., Banerjee, P., McDonald, D., and Martonchik, J.: Aerosol properties derived from aircraft multiangle imaging over Monterey Bay, J. Geophys. Res., 106, 11977–11995, 2001b.

AMTD
7, 7837–7882, 2014

Kahn, R. A., Li, W.-H., Martonchik, J. V., Bruegge, C. J., Diner, D. J., Gaitley, B. J., and Abdou, W.: MISR calibration and implications for low-light-level aerosol retrieval over dark water, J. Atmos. Sci., 62, 1032–1052, 2005a.

Kahn, R. A., Gaitley, B., Martonchik, J., Diner, D., Crean, K., and Holben, B.: MISR global aerosol optical depth validation based on two years of coincident AERONET observations, J. Geophys. Res., 110, D10S04, doi:10.1029/2004JD004706, 2005b.

Kahn, R. A., Garay, M. J., Nelson, D. L., Yau, K. K., Bull, M. A., Gaitley, B. J., Martonchik, J. V., and Levy, R. C.: Satellite-derived aerosol optical depth over dark water from MISR and MODIS: comparisons with AERONET and implications for climatological studies, J. Geophys. Res., 112, D18205, doi:10.1029/2006JD008175, 2007.

Kahn, R. A., Nelson, D. L., M.Garay, Levy, R. C., Bull, M. A., Martonchik, J. V., Diner, D. J., Paradise, S. R., and Hansen, E. G., and Remer, L. A.: MISR Aerosol product attributes, and statistical comparison with MODIS, IEEE T. Geosci. Remote, 47, 4095–4114, 2009.

Kahn, R. A., Gaitley, B. J., Garay, M. J., Diner, D. J., Eck, T., Smirnov, A., and Holben, B. N.: Multiangle Imaging SpectroRadiometer global aerosol product assessment by comparison with the Aerosol Robotic Network, J. Geophys. Res., 115, D23209, doi:10.1029/2010JD014601, 2010.

Kahn, R. A., Garay, M. J., Nelson, D. L., Levy, R. C., Bull, M. A., Diner, D. J., Martonchik, J. V., Hansen, E. G., Remer, L. A., and Tanré, D.: Response to "Toward unified satellite climatology of aerosol properties. 3. MODIS versus MISR versus AERONET", J. Quant. Spectrosc. Ra., 112, 901–909, doi:10.1016/j.jqsrt.2009.11.003, 2011.

Kalashnikova, O. V., Kahn, R., Sokolik, I. N., and Li, W.-H.: The ability of multi-angle remote sensing observations to identify and distinguish mineral dust types: Part 1. Optical models and retrievals of optically thick plumes, J. Geophys. Res., 110, D18S14, doi:10.1029/2004JD004550, 2005.

Kokhanovsky, A. A., Deuzé, J. L., Diner, D. J., Dubovik, O., Ducos, F., Emde, C., Garay, M. J., Grainger, R. G., Heckel, A., Herman, M., Katsev, I. L., Keller, J., Levy, R., North, P. R. J., Prikhach, A. S., Rozanov, V. V., Sayer, A. M., Ota, Y., Tanré, D., Thomas, G. E., and Zege, E. P.: The inter-comparison of major satellite aerosol retrieval algorithms using simulated intensity and polarization characteristics of reflected light, Atmos. Meas. Tech., 3, 909–932, doi:10.5194/amt-3-909-2010, 2010.

Koepke, P.: Effective reflectance of oceanic whitecaps, Appl. Optics, 23, 1816, doi:10.1364/AO.23.001816, 1984.

AMTD
7, 7837–7882, 2014

Li, S., Kahn, R. A., Chin, M., Garay, M. J., and Liu, Y.: Improving MISR retrieved aerosol microphysical properties using GoCART data, Atmos. Meas. Tech. Discuss., in preparation, 2014.

Maritorena, S. and Siegel, D. A.: Consistent merging of satellite ocean color data sets using a bio-optical model, Remote Sens. Environ., 94, 429–440, 2005.

Martonchik, J. V., Diner, D. J., Kahn, R., Verstraete, M. M., Pinty, B., Gordon, H. R., and Ackerman, T. P.: Techniques for the Retrieval of aerosol properties over land and ocean using multiangle imaging, IEEE T. Geosci. Remote, 36, 1212–1227, 1998.

Martonchik, J. V., Diner, D. J., Crean, K., and Bull, M.: Regional aerosol retrieval results from MISR, IEEE T. Geosci. Remote, 40, 1520–1531, 2002.

Martonchik, J. V., Kahn, R. A., and Diner, D. J.: Retrieval of aerosol properties over land using MISR observations, in: Satellite Aerosol Remote Sensing Over Land, edited by: Kokhanovsky, A., Springer, Berlin, 267–293, 2009.

Monahan, E. C. and O'Muircheartaigh, I. G.: Optimal power-law description of oceanic whitecap coverage dependence on wind speed, J. Phys. Oceanogr., 10, 2094, doi:10.1175/1520-0485(1980)010<2094:OPLDOO>2.0.CO;2, 1980.

Pierce, J. R., Kahn, R. A., Davis, M. R., and Comstock, J. M.: Detecting thin cirrus in Multiangle Imaging Spectroradiometer aerosol retrievals, J. Geophys. Res., 115, D08201, doi:10.1029/2009JD013019, 2010.

Sayer, A. M., Thomas, G. E., and Grainger, R. G.: A sea surface reflectance model for (A)ATSR, and application to aerosol retrievals, Atmos. Meas. Tech., 3, 813–838, doi:10.5194/amt-3-813-2010, 2010.

Shi, Y., Zhang, J., Reid, J. S., Liu, B., and Hyer, E. J.: Critical evaluation of cloud contamination in the MISR aerosol products using MODIS cloud mask products, Atmos. Meas. Tech., 7, 1791–1801, doi:10.5194/amt-7-1791-2014, 2014.

Smirnov, A., Holben, B. N., Slutsker, I., Giles, D. M., McClain, C. R., Eck, T. F., Sakerin, S. M., Macke, A., Croot, P., Zibordi, G., Quinn, P. K., Sciare, J., Kinne, S., Harvey, M., Smyth, T. J., Piketh, S., Zielinski, T., Proshutinsky, A., Goes, J. I., Nelson, N. B., Larouche, P., Radionov, V. F., Goloub, P., Krishna Moorthy, K., Matarrese, R., Robertson, E. J., and Jourdin, F.: Maritime Aerosol Network as a component of Aerosol Robotic Network, J. Geophys. Res., 114, D06204, doi:10.1029/2008JD011257, 2009.

Voss, K. J. and Chapin, A. L.: Upwelling radiance distribution camera system, NURADS, Opt. Express, 13, 4250–4262, 2005.

AMTD
7, 7837–7882, 2014

Witek, M. L., Garay, M. J., Diner, D. J., and Smirnov, A.: Aerosol optical depths over oceans: a view from MISR retrievals and collocated MAN and AERONET in-situ observations, J. Geophys. Res, 118, 12620–12633, doi:10.1002/2013JD020393, 2013.

AMTD
7, 7837–7882, 2014

Table 1. Dimensions of the MISR RA Look-up Table (LUT), representing the SMART output.

Variable	Description	Values
μ_0	cos (sun zenith angle)	0.2–0.9 (in 0.05 increments); 0.925, 0.95, 0.975, 0.99, 1.0
μ	cos (view zenith angle)	0.31, 0.33, 0.35; 0.47, 0.49, 0.51; 0.66, 0.685, 0.71; 0.84, 0.87, 0.9; 0.95, 0.975, 0.99, 1.0
τ	Spectral AOD	0, 0.05, 0.1, 0.2, 0.35, 0.55, 0.75, 1.0, 1.5, 2, 3, 5, 7, 9.5
P	Surf. Pressure (mb)	607.95, 1050.0
u	Surf. Wind Speed ($m\,s^{-1}$)	0.5, 5.0, 7.5, 10.0, 12.5
λ	Spectral Band (nm)	446 (blue), 558 (green), 672 (red), 866 (NIR)
Θ^*	Scattering Angle	0.0 (minimum) – 180.0 (maximum). Scattering angle range varies based on μ_0, μ.
m	Aerosol Mixture	74 (Kahn et al., 2010) or 774 (Tables 3 and 4)

* Scattering Angle grids (a grid for each $\mu - \mu_0$ combination) were selected so maximum errors in the interpolated LUT values do not exceed 1 % of the value compared to a 1° resolution scattering angle grid. For view zenith angle, triplets allow for changes in viewing zenith in the across-track direction. View zenith angle changes by about 17° across-track for the nadir camera.

AMTD
7, 7837–7882, 2014

Table 2. Number of MISR-AERONET and MISR-MAN validation cases, stratified by fraction-not-clear and Chlorophyll *a* concentration.

Condition*	AERONET	MAN
FNC < 0.05		
$C < 0.25$	93	19
$0.25 \leq C \leq 0.5$	19	4
$C > 0.5$	13	16
$0.05 \leq$ FNC ≤ 0.75		
$C < 0.25$	658	75
$0.25 \leq C \leq 0.5$	95	14
$C > 0.5$	37	16
FNC > 0.75	39	14
Total	954	178

* FNC = 3 × 3 retrieval average Fraction not clear; C = 3 × 3 retrieval average Chlorophyll *a* concentration (mg m^{-3}).

AMTD
7, 7837–7882, 2014

MISR Research-Aerosol-Algorithm: refinements for dark water retrievals

J. A. Limbacher and R. A. Kahn

Table 3. MISR components for the 774-mixture set*.

Component Name	r_1 (μm)	r_2 (μm)	r_e (μm)	σ	E(B/G)	E(R/G)	E(NIR/G)	n_r(G)	SSA(B)	SSA(G)	SSA(R)	SSA(NIR)	g(G)
sph_nonabs_0.06	0.002	0.329	0.056	1.650	1.947	0.548	0.226	1.520	1.000	1.000	1.000	1.000	0.357
sph_nonabs_0.12	0.003	0.747	0.121	1.700	1.512	0.669	0.357	1.500	1.000	1.000	1.000	1.000	0.597
sph_nonabs_0.26	0.005	1.690	0.262	1.750	1.185	0.820	0.576	1.450	1.000	1.000	1.000	1.000	0.717
sph_nonabs_0.57	0.008	3.805	0.568	1.800	0.993	0.972	0.877	1.410	1.000	1.000	1.000	1.000	0.750
sph_nonabs_1.28	0.013	8.884	1.285	1.850	0.956	1.039	1.082	1.370	1.000	1.000	1.000	1.000	0.769
sph_abs_0.12_0.80_flat	0.003	0.747	0.121	1.700	1.461	0.687	0.378	1.500	0.818	0.822	0.825	0.828	0.604
sph_abs_0.12_0.80_steep	0.003	0.747	0.121	1.700	1.453	0.698	0.403	1.500	0.838	0.822	0.801	0.756	0.604
sph_abs_0.12_0.90_flat	0.003	0.747	0.121	1.700	1.488	0.677	0.367	1.500	0.910	0.912	0.913	0.915	0.601
sph_abs_0.12_0.90_steep	0.003	0.747	0.121	1.700	1.484	0.683	0.379	1.500	0.920	0.912	0.900	0.875	0.601
dust_grains_mode1_h1	0.100	1.000	0.754	1.500	0.895	1.065	1.079	1.510	0.920	0.977	0.994	0.997	0.711
spheroidal_mode2_h1	0.100	6.000	2.400	2.000	0.989	1.019	1.050	1.510	0.810	0.902	0.971	0.983	0.772
baum_cirrus_De = 10 μm	2.000	9500.000	5.000	n/a	1.000	1.000	1.000	1.317	1.000	1.000	1.000	1.000	0.787
baum_cirrus_De = 40 μm	2.000	9500.000	20.000	n/a	1.000	1.000	1.000	1.317	1.000	1.000	1.000	1.000	0.810
baum_cirrus_De = 100 μm	2.000	9500.000	50.000	n/a	1.000	1.000	1.000	1.317	1.000	1.000	1.000	1.000	0.869

* r_1, r_2 are the upper and lower limits of the component particle size distribution; r_e is effective radius (μm), σ is the log-normal size distribution width, E is the spectral ratio of extinction cross-section, g is the asymmetry parameter; dust grain and spheroid optical properties from Kalashnikova et al. (2005); cirrus from Baum et al. (2005).

AMTD
7, 7837–7882, 2014

Table 4. Mixing groups comprising the 774-mixture set.

Component 1	Component 2	Component 3
spherical_nonabsorbing_0.06	spherical_nonabsorbing_1.28	spherical_nonabsorbing_0.57
spherical_nonabsorbing_0.12	spherical_nonabsorbing_1.28	spherical_nonabsorbing_0.57
spherical_nonabsorbing_0.26	spherical_nonabsorbing_1.28	spherical_nonabsorbing_0.57
spherical_nonabsorbing_0.06	dust_grains_mode1_h1	spheroidal_mode2_h1
spherical_nonabsorbing_0.12	dust_grains_mode1_h1	spheroidal_mode2_h1
spherical_nonabsorbing_0.26	dust_grains_mode1_h1	spheroidal_mode2_h1
spherical_nonabsorbing_0.06	spherical_nonabsorbing_1.28	dust_grains_mode1_h1
spherical_nonabsorbing_0.12	spherical_nonabsorbing_1.28	dust_grains_mode1_h1
spherical_nonabsorbing_0.26	spherical_nonabsorbing_1.28	dust_grains_mode1_h1
spherical_absorbing_0.12_0.80_steep	spherical_nonabsorbing_1.28	dust_grains_mode1_h1
spherical_absorbing_0.12_0.80_flat	spherical_nonabsorbing_1.28	dust_grains_mode1_h1
spherical_absorbing_0.12_0.90_steep	spherical_nonabsorbing_1.28	dust_grains_mode1_h1
spherical_absorbing_0.12_0.90_flat	spherical_nonabsorbing_1.28	dust_grains_mode1_h1
baum_cirrus_De = 10 µm	–	–
baum_cirrus_De = 40 µm	–	–
baum_cirrus_De = 100 µm	–	–

AMTD
7, 7837–7882, 2014

Table 5. Statistics of AOD and ANG retrievals stratified by adjustment*.

Adjustment (Blue)	0.05 or 20%	0.03 or 10%	Std	RMSE	MAE	Med Bias	#
SA Control	62	37	0.059	0.074	0.043	0.038	1121
SA + 0.5 NCF	68	42	0.054	0.065	0.037	0.032	979
RA Control	70	45	0.058	0.065	0.036	0.026	1132
RA + Median or Min	72	47	0.056	0.061	0.035	0.023	1132
RA + Ocean Surface	76	53	0.058	0.059	0.029	0.014	1132
RA + Mixtures	78	53	0.051	0.054	0.030	0.018	1132
RA + All Adj.	83	61	0.047	0.048	0.024	0.008	1121
RA + All Adj. + 0.5 NCF	**87**	**66**	**0.045**	**0.045**	**0.021**	**0.003**	**979**
Adjustment (Green)	0.05 or 20%	0.03 or 10%	Std	RMSE	MAE	Med Bias	#
SA Control	75	51	0.048	0.056	0.030	0.026	1121
SA + 0.5 NCF	80	59	0.043	0.048	0.026	0.020	979
RA Control	80	57	0.046	0.051	0.027	0.019	1132
RA + Median or Min	82	58	0.044	0.047	0.026	0.016	1132
RA + Ocean Surface	83	60	0.046	0.048	0.024	0.014	1132
RA + Mixtures	83	61	0.043	0.046	0.025	0.016	1132
RA + All Adj.	86	67	0.040	0.041	0.021	0.009	1121
RA + All Adj. + 0.5 NCF	**89**	**73**	**0.037**	**0.037**	**0.018**	**0.004**	**979**
Adjustment (Red)	0.05 or 20%	0.03 or 10%	Std	RMSE	MAE	Med Bias	#
SA Control	82	62	0.042	0.047	0.024	0.019	1121
SA + 0.5 NCF	88	69	0.036	0.039	0.021	0.013	979
RA Control	85	64	0.040	0.044	0.023	0.015	1132
RA + Median or Min	86	66	0.037	0.040	0.021	0.012	1132
RA + Ocean Surface	85	66	0.039	0.042	0.021	0.013	1132
RA + Mixtures	84	64	0.039	0.043	0.022	0.015	1132
RA + All Adj.	88	72	0.036	0.037	0.019	0.009	1121
RA + All Adj. + 0.5 NCF	**92**	**76**	**0.033**	**0.033**	**0.017**	**0.004**	**979**
Adjustment (NIR)	0.05 or 20%	0.03 or 10%	Std	RMSE	MAE	Med Bias	#
SA Control	88	69	0.037	0.040	0.019	0.013	1121
SA + 0.5 NCF	92	77	0.032	0.033	0.016	0.007	979
RA Control	87	69	0.036	0.039	0.020	0.012	1132
RA + Median or Min	89	71	0.034	0.035	0.018	0.009	1132
RA + Ocean Surface	86	68	0.036	0.039	0.020	0.013	1132
RA + Mixtures	86	67	0.036	0.040	0.020	0.015	1132
RA + All Adj.	90	74	0.033	0.035	0.018	0.010	1121
RA + All Adj. + 0.5 NCF	**93**	**80**	**0.029**	**0.030**	**0.015**	**0.005**	**979**
Adjustment (ANG)	0.5	0.275	Std	RMSE	MAE	Med Bias	#
SA Control	78	49	0.397	0.448	0.279	0.214	1117
SA + 0.5 NCF	76	47	0.386	0.454	0.296	0.237	976
RA Control	79	55	0.462	0.472	0.246	0.062	1128
RA + Median or Min	78	53	0.467	0.481	0.253	0.081	1128
RA + Ocean Surface	83	59	0.424	0.434	0.224	-0.078	1128
RA + Mixtures	87	65	0.387	0.389	0.187	-0.034	1128
RA + All Adj.	87	68	0.369	0.377	0.178	-0.044	1117
RA + All Adj. + 0.5 NCF	**86**	**67**	**0.360**	**0.366**	**0.182**	**-0.039**	**976**

* Columns 2 and 3 give the percent of validation cases within the confidence envelopes indicated, STD is the standard deviation, RMSE is the root-mean-square error, MAE is the mean absolute error, Med Bias is the median bias, and # is the number of validation cases included. The first four data blocks give the spectral AOD statistics, and the fifth data block presents the ANG statistics.

AMTD
7, 7837–7882, 2014

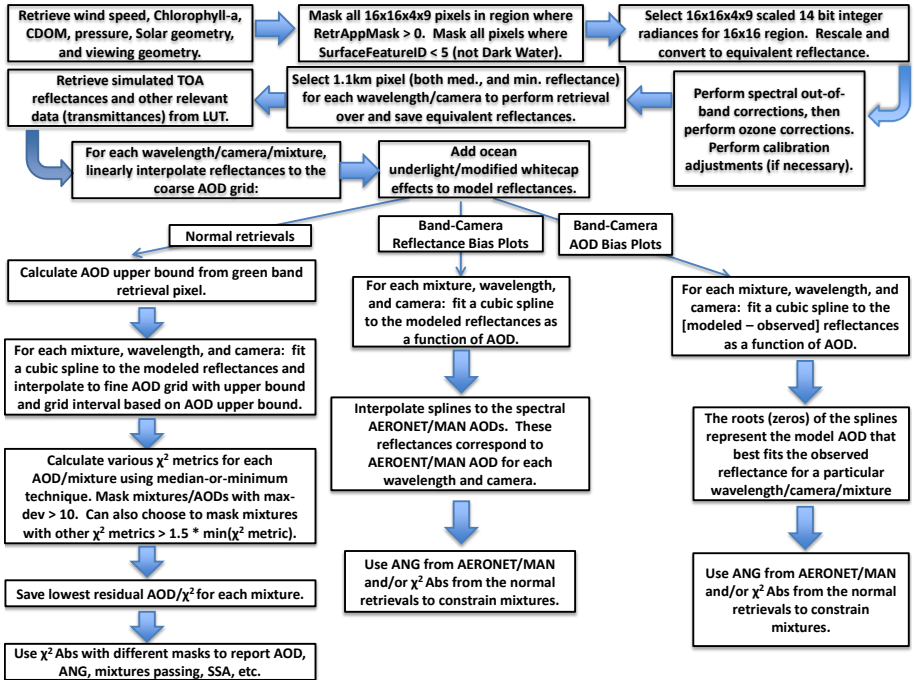

Figure 1. Flow chart summarizing the steps involved in Research Algorithm aerosol retrievals over dark water.

AMTD
7, 7837–7882, 2014

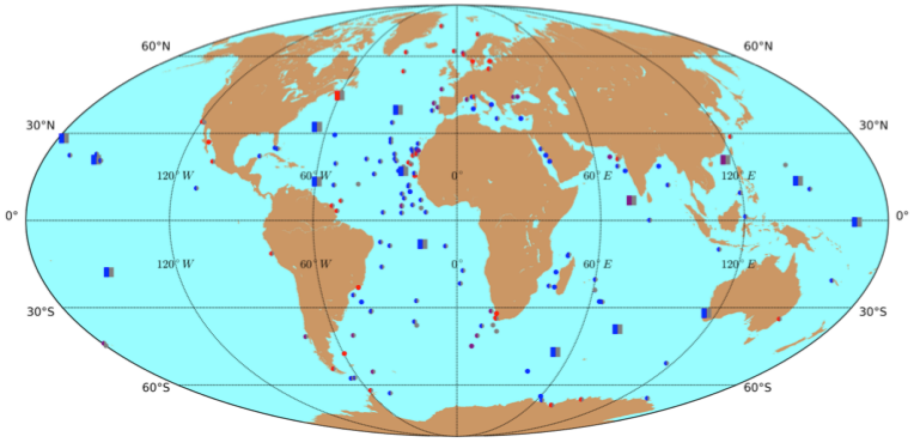

Figure 2. Map showing the geographical distribution of 954 MISR-AERONET and 178 MISR-MAN validation cases. Squares are used for AERONET sites and circles for MAN. A fully shaded gray marker indicates fraction-not-clear (FNC) > 0.75, whereas a partly shaded grey marker indicates FNC in the range 0.05–0.75. If no gray is used, the location has FNC < 0.05. Blue markers indicate an average Chlorophyll *a* concentration (C) of $< 0.25\,\mathrm{mg\,m^{-3}}$, purple indicates C between 0.25 and $0.5\,\mathrm{mg\,m^{-3}}$, and red indicates $C > 0.5\,\mathrm{mg\,m^{-3}}$.

AMTD
7, 7837–7882, 2014

MISR Research-Aerosol-Algorithm: refinements for dark water retrievals

J. A. Limbacher and R. A. Kahn

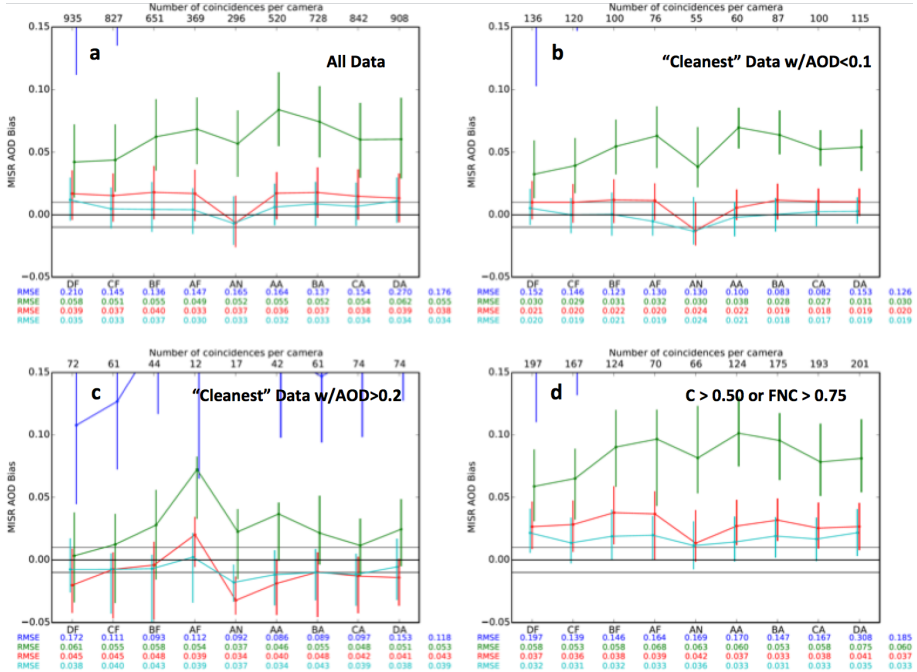

Figure 3. Baseline case bias plots. These panels show the bias in each MISR channel for: **(a)** All data, **(b)** AOD < 0.10, C < 0.25, and FNC < 0.05, **(c)** AOD > 0.20, C < 0.25, and FNC < 0.05, and **(d)** C > 0.50 or FNC > 0.75. The points represent the median values for each particular wavelength and camera; the vertical bars represent the 25th–75th percentiles. The count is shown for each channel near the top of the plot, and the RMSE (for each camera and wavelength) is shown near the bottom. The numbers on the right represent the camera-averaged values for the RMSE. Median values in the blue band are off-scale for nearly all cameras.

AMTD
7, 7837–7882, 2014

MISR Research-Aerosol-Algorithm: refinements for dark water retrievals

J. A. Limbacher and R. A. Kahn

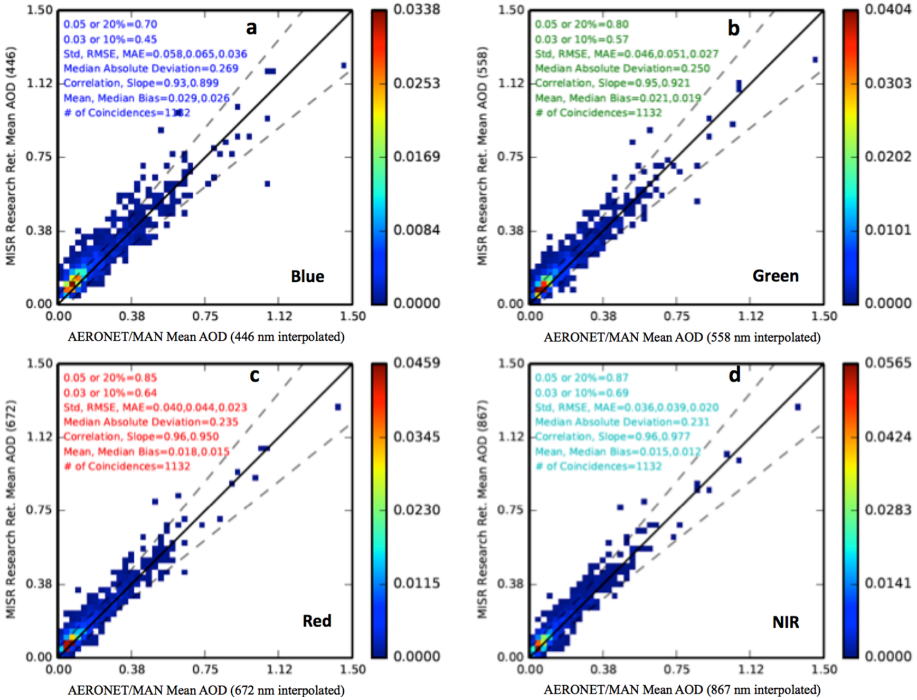

Figure 4. Baseline case scatter-density plots. These panels present the joint PDF of MISR-AERONET/MAN data for the four MISR wavelengths: **(a)** blue, **(b)** green, **(c)** red, **(d)** NIR. The first number in the upper left of each plot gives the fraction of points that fall within 0.05 or 20 % of the AERONET/MAN interpolated AOD. The second number represents the fraction that falls within 0.03 or 10 % of the AERONET/MAN interpolated value. The standard deviation shown for each plot is calculated for the MISR-AERONET/MAN AOD differences. The RMSE is reported with the AERONET/MAN value used as the expected value. MAE is the median absolute error. The mean and median biases are the average biases reported over all coincidences.

AMTD
7, 7837–7882, 2014

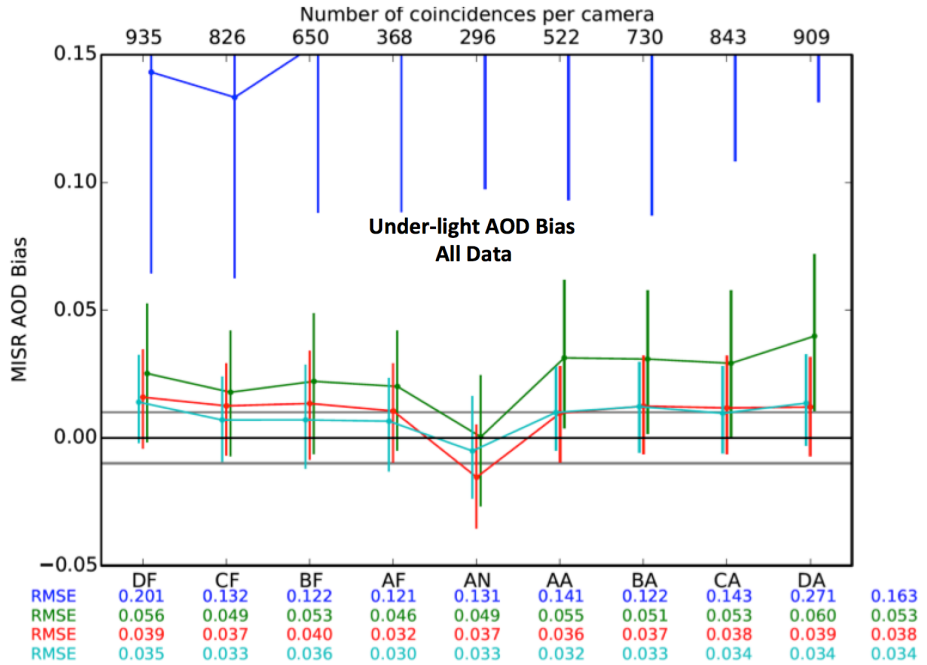

Figure 5. Channel-by-channel MISR AOD biases including all validation data, when the under-light and modified whitecap representations are applied.

AMTD
7, 7837–7882, 2014

MISR Research-Aerosol-Algorithm: refinements for dark water retrievals

J. A. Limbacher and R. A. Kahn

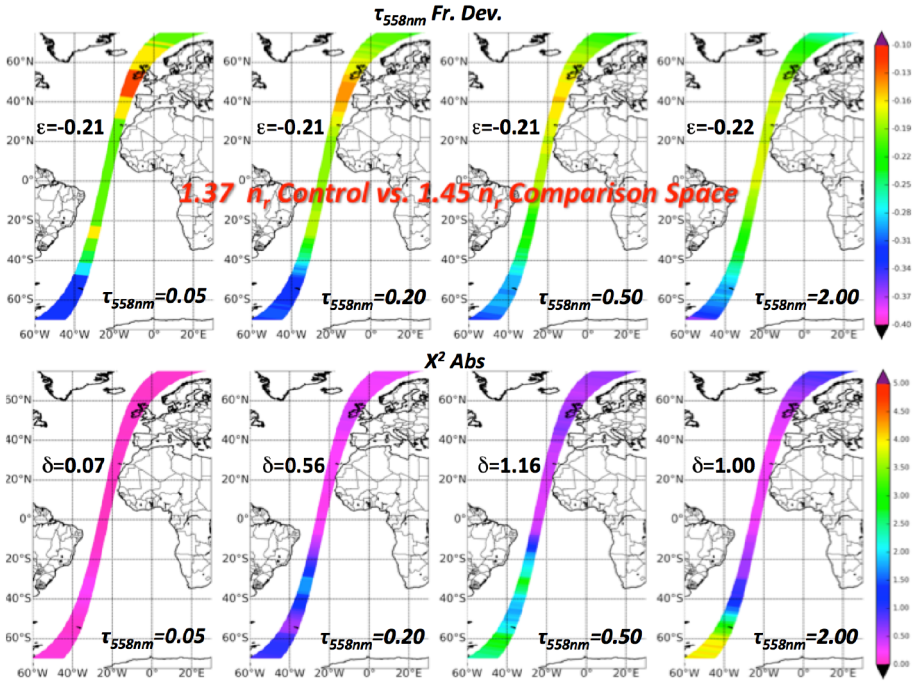

Figure 6. Real refractive index theoretical sensitivity study. The top four panels show the fractional change in retrieved AOD for an atmosphere containing 1.28 micron non-absorbing particles with n_r = 1.37, when the comparison space contains the same particle but with n_r = 1.45, for 558 nm control AOD values of 0.05, 0.20, 0.50, and 2.0. The bottom four panels present the χ^2_{abs} values for the lowest residual retrieved AOD for the same four control AOD values. As values vary with retrieval geometry, results are plotted for an illustrative orbit, orbit 70499, 20 March 2013. Over-water conditions are assumed everywhere, with the surface pressure prescribed as 1013.25 mbar, and the surface wind speed set to 2.5 m s^{-1}. The orbit-mean fractional changes in AOD (ε) and χ^2_{abs} (δ) values are indicated in each upper or lower panel, respectively.

AMTD
7, 7837–7882, 2014

MISR Research-Aerosol-Algorithm: refinements for dark water retrievals

J. A. Limbacher and R. A. Kahn

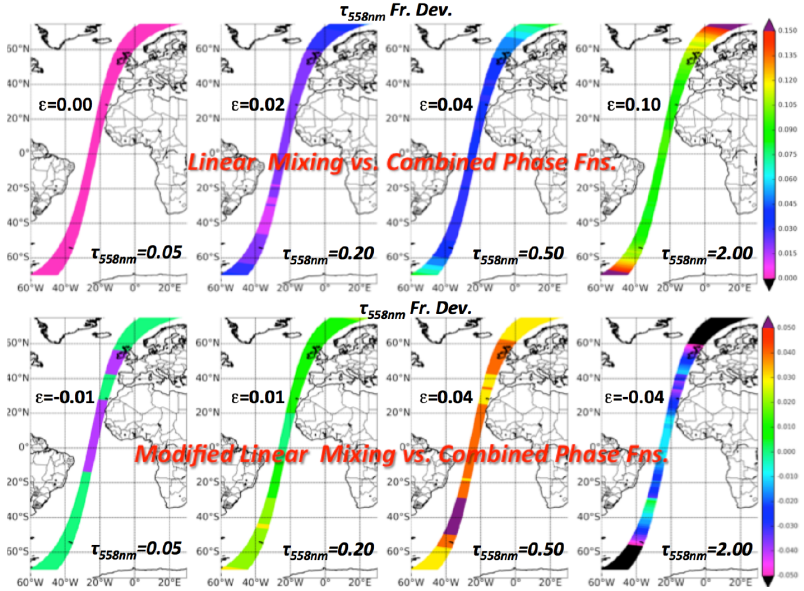

Figure 7. Modified Linear Mixing (MLM) theoretical sensitivity study, showing the fractional change in retrieved AOD for a two-aerosol-component atmosphere containing spherical particles having r_e = 1.28 and 0.06 micron, 50 % mid-visible AOD each. The top four panels show the fractional retrieved-AOD change when both components are non-absorbing and a linear mixing approximation is used to combine the particles rather than mixing the phase functions according to Eq. (2). The bottom four panels show the fractional change in retrieved AOD when the modified linear mixing approximation is used to combine a 1.28 micron non-absorbing particle with a 0.06 micron absorbing particle, having SSA = 0.80 at a wavelength of 558 nm, rather than mixing the phase functions. For both sets of panels, the total-column AOD values at 558 nm are 0.05, 0.20, 0.50, and 2.0. The orbit-mean AOD error (ε) is indicated in each panel. The viewing and solar geometry for these forward model runs correspond to orbit 70499, 20 March 2013. Only over-water retrievals were performed, with the surface pressure prescribed as 1013.25 mbar, and the surface wind speed set to 2.5 m s^{-1}.

AMTD
7, 7837–7882, 2014

MISR Research-Aerosol-Algorithm: refinements for dark water retrievals

J. A. Limbacher and R. A. Kahn

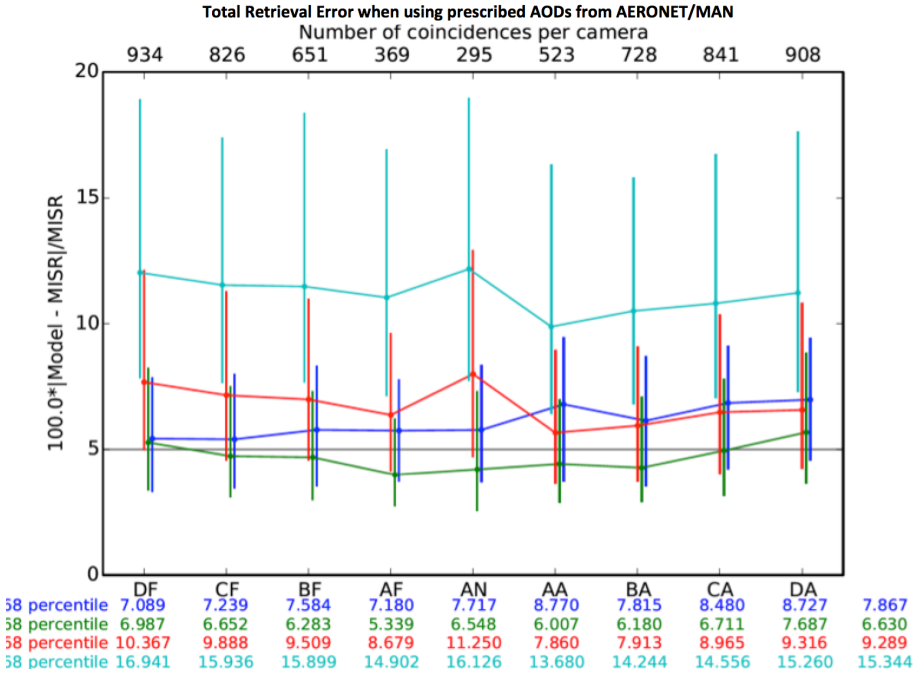

Figure 8. Total fractional retrieval error in TOA reflectance (Eq. 3) when using the prescribed AODs from AERONET/MAN. Instead of showing the RMSEs at the bottom, the 68th percentile values are indicated.

AMTD
7, 7837–7882, 2014

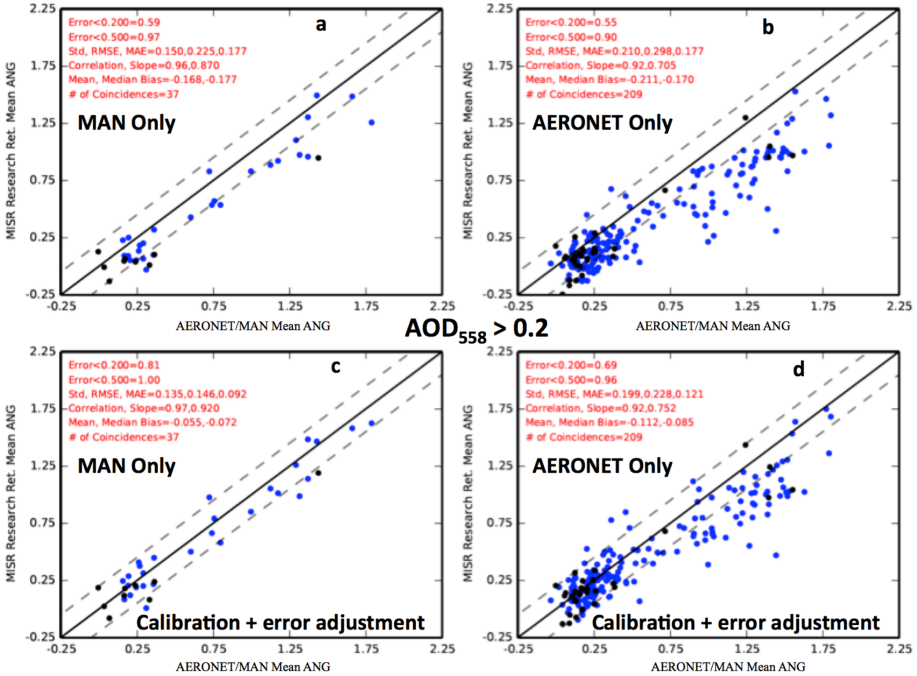

Figure 9. Scatter-plots showing MISR vs. AERONET/MAN ANG data for AOD > 0.20, with all modifications **(c, d)** and with all modifications except the calibration corrections and the error adjustment **(a, b)**. The MISR-MAN coincidences are given in **(a)** and **(c)**, and the MISR-AERONET coincidences correspond to **(b)** and **(d)**. Blue dots represent coincidences with a MAN/AERONET 558 nm AOD of between 0.2 and 0.5. Black dots represent coincidences with AERONET/MAN AOD values > 0.5.

AMTD
7, 7837–7882, 2014

MISR Research-Aerosol-Algorithm: refinements for dark water retrievals

J. A. Limbacher and R. A. Kahn

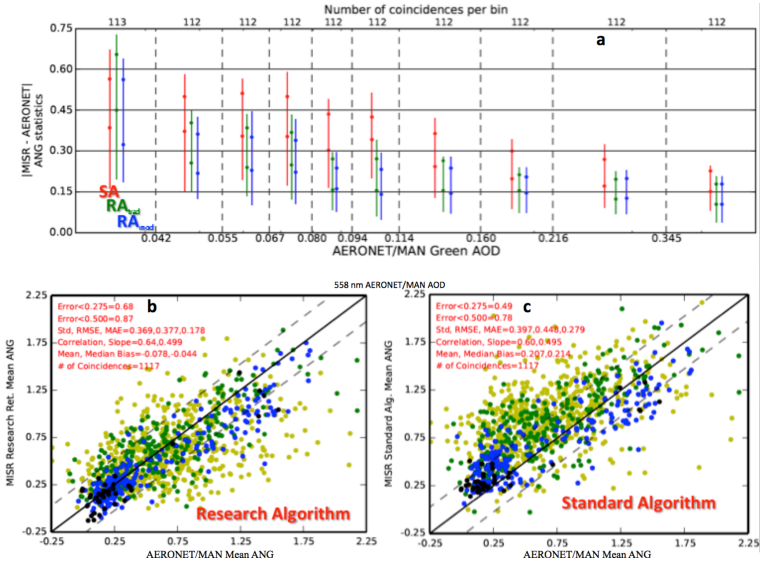

Figure 10. (a) shows the statistics of the |MISR-MAN/AERONET| Ångström exponent coincidences, conditioned on 558 nm AERONET/MAN AOD. The first line of the triplets shows the SA-AERONET/MAN comparison, the second line shows the comparison between the RA and MISR-MAN/AERONET with the standard abs criterion, and the 3rd line shows the comparison between the RA and MISR-MAN/AERONET with the modified abs criterion. The vertical lines represent the 25th–75th percentiles, while the lower dot represents the median absolute error. The upper dot represents the 68th percentile value. The x axis is logged so that the data are easier to present, and the number of coincidences per AOD bin is listed at the top. The upper limit of each AOD bin (green band, binning is done based on green band AOD) is shown at the bottom (except for the last AOD bin). **(b)** (Research Algorithm, all modifications with updated chisq criterion) and **(c)** (Standard Algorithm) show the MISR-AERONET/MAN ANG cases for all AOD > 0.01. Yellow dots correspond to points with AERONET AOD less than 0.10, green dots indicate an AOD between 0.10 and 0.20, blue dots indicate an AOD between 0.20 and 0.50, and black dots indicate an AOD greater than 0.50.

AMTD
7, 7837–7882, 2014

MISR Research-Aerosol-Algorithm: refinements for dark water retrievals

J. A. Limbacher and R. A. Kahn

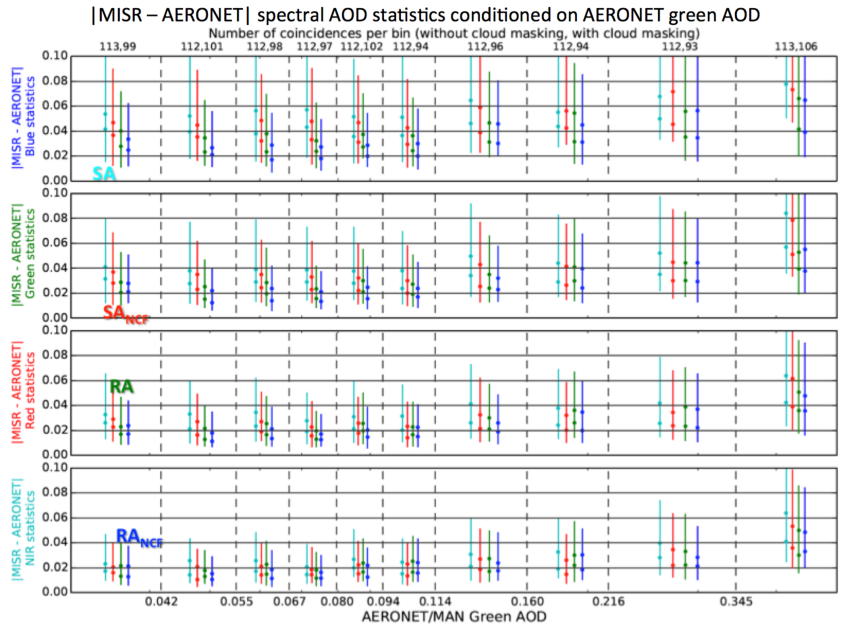

Figure 11. |MISR-AERONET| spectral AOD statistics conditioned on AERONET green AOD. For the vertical lines/points: cyan represents the SA, red represents the SA with enhanced cloud screening (NCF < 0.50), green represents the RA with all modifications through Sect. 4.2, and blue represents the RA with all modifications and enhanced cloud screening (NCF < 0.50). The vertical lines indicate the 25th–75th percentiles, and the lower dot gives the median absolute error. The upper dot represents the 68th percentile value. Each row of plots presents results for one of the four MISR spectral bands (blue, green, red, and NIR). The number of coincidences per AOD bin is listed at the top (both without and with enhanced cloud masking). Vertical dashed lines separate AOD bins, which are defined based on the green band AOD. The upper limit of each (green band) AOD bin is shown at the bottom (except for the last AOD bin). The *x* axis is logged so that the data are easier to present.

AMTD
7, 7837–7882, 2014

MISR Research-Aerosol-Algorithm: refinements for dark water retrievals

J. A. Limbacher and R. A. Kahn